nature communications

Article

https://doi.org/10.1038/s41467-025-63953-7

Paraventricular nucleus CRH neurons regulate acute lung injury via sympathetic nerve–neutrophil axis

Received: 23 January 2025

Accepted: 28 August 2025

Published online: 06 October 2025

Check for updates

Hui Li[1,2,5] ✉, Tao Liu[1,2,5], Yang Wang[1,2], Xue-Mei Miao[1,2], Yi-Yu Xiong[1,2], Qian Zhao[1,2], Wei-Yun Shen[1,2], Fu-Hong Su[3], Kang Chen[4] & Ru-Ping Dai[1,2] ✉

Acute lung injury (ALI) and acute respiratory distress syndrome (ARDS) are severe conditions with high morbidity and mortality with limited effective therapies. Neuroimmune interactions play a critical role in lung homeostasis, but it remains unclear if specific brain regions regulate lung inflammation. Here, we perform anatomical tracing, chemogenetic modulation, and pharmacological interventions in male mice and identify a neural circuit from corticotropin-releasing hormone neurons in the paraventricular nucleus of the hypothalamus (CRH^{PVN} neurons) to the lung. The activation of these neurons protects mice from ALI and promotes survival, reduces neutrophil infiltration and effector functions in the lung, whereas inhibiting CRH^{PVN} neurons worsens ALI. The protective effect is mediated by increased sympathetic nervous activity, with locally released norepinephrine modulating neutrophil functions via β2-AR–β-arrestin2 signaling to inhibit the NF-κB pathway. These findings uncover a brain-lung neural circuit that modulates immune responses during ALI, offering a potential therapeutic target for ALI and ARDS.

Acute lung injury (ALI) and ensuing acute respiratory distress syndrome (ARDS) are inflammatory disease syndromes of the lung that are characterized by the flooding of the alveoli with protein- and leukocyte-rich edema as a result of a direct injury to the lung, such as in sepsis[1–4]. Treatments of ALI are limited in part due to the complex nature of lung inflammatory response, which involves delicate interaction of different types of cells, including lung neurons[5]. In light of the fact that neuroimmune pathways are critical for the maintenance of airway functions and amenable to rapid modulation[6–8], we sought to elucidate the neuroimmune pathways that regulate lung inflammation to identify strategies to rapidly and effectively alleviate or treat ALI and other related pathological conditions.

In addition to local neuro-lung interactions involving neurons that innervate the lung[9–12], the brain at subcortical sites, such as the hypothalamus or nucleus solitary tract (NTS), receives interoceptive information from the lungs and exerts reflexive control that elicits a hard-wired neuro-lung response. For example, chronic allergen insults to the airway are transmitted via ascending vagal afferents to the dopamine beta-hydroxylase-expressing ($D\beta h^{+}$) NTS integrator, which then descends through efferent choline acetyltransferase-positive neurons in the nucleus ambiguus ($Chat^{+}$ NA neurons) to drive airway hyperreactivity[13]. Moreover, the activation of transient receptor potential vanilloid 1 ($TRPV1^{+}$) nociceptor in the lung induces acute stress responses in the hypothalamus by activating corticotropin-releasing hormone (CRH) neurons in the paraventricular nucleus (PVN) (CRH^{PVN}), which are responsible for sickness behaviors[14]. However, it is still unknown whether and how the brain perceives and influences inflammatory signals in the lung in the progression of ALI.

Here, using whole-brain mapping and fiber photometric recording, we observed profound activation of CRH^{PVN} neurons associated with lung injury. Virus neuronal tracing found that CRH^{PVN} neurons

[1]Department of Anesthesiology, The Second Xiangya Hospital, Central South University, Changsha, China. [2]Anesthesiology Research Institute, Central South University, Changsha, China. [3]Department of Intensive Care, Erasmus Hospital, Brussels, Belgium. [4]Department of Obstetrics and Gynecology, Wayne State University, Detroit, MI, USA. [5]These authors contributed equally: Hui Li, Tao Liu. ✉e-mail: lihui_1166@csu.edu.cn; xyeyyrupingdai@csu.edu.cn

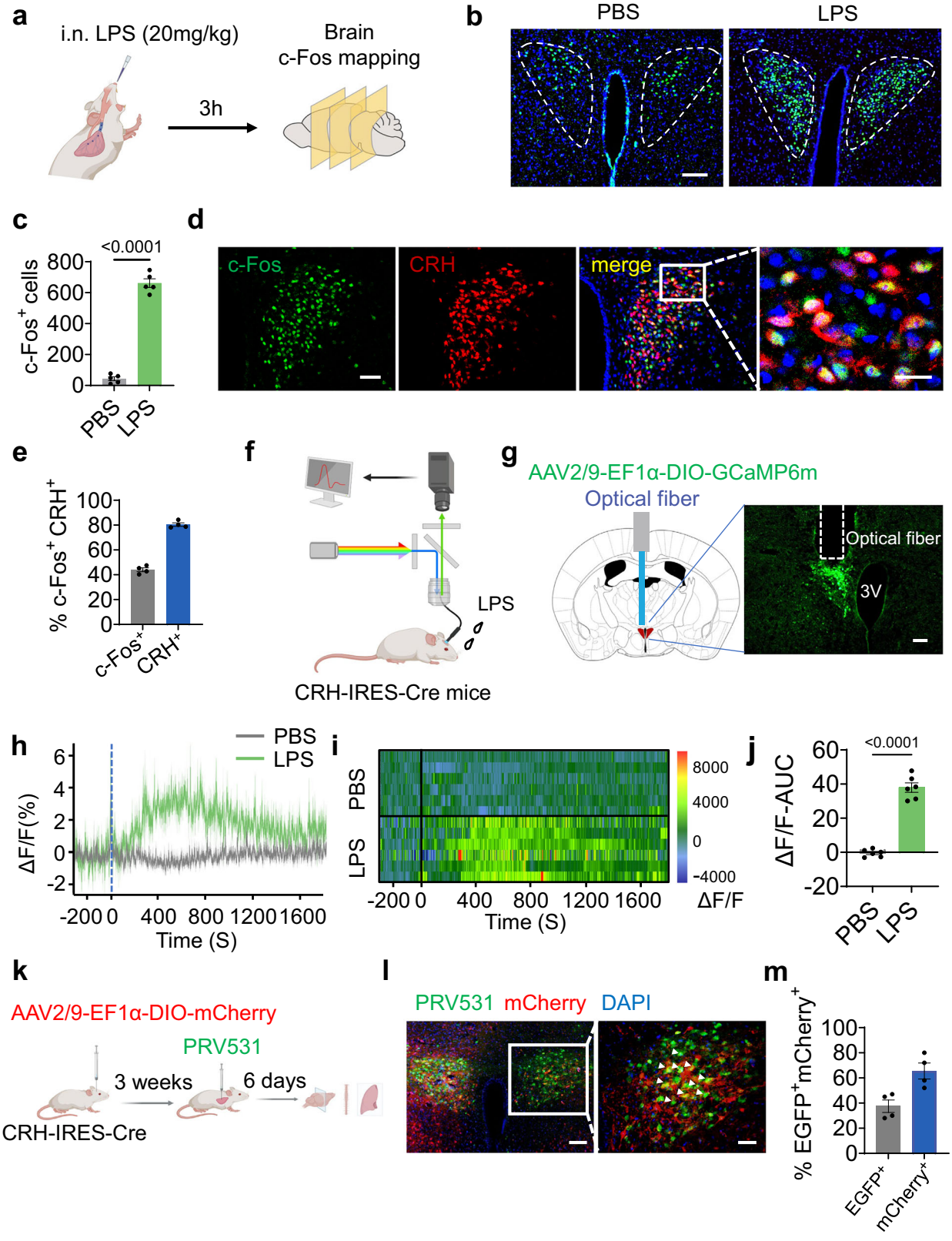

were directly connected to the lung. Chemogenetic activation of CRH^{PVN} neurons in mice subjected to ALI reduced mortality and mitigated lung inflammation and neutrophil infiltration into the lung, accompanied by a marked increase in lung sympathetic activity. Conversely, the inhibition of CRH^{PVN} neurons exacerbated ALI and neutrophil accumulation in the lung. Chemical sympathectomy or β_2 adrenergic receptor (β_2-AR) blockade in the lung abolished the protective effect of CRH^{PVN} neuronal activation. The sympathetic neurotransmitter norepinephrine (NE) restricted lung neutrophil inflammation and effector function via β_2-AR–β-arrestin2 signaling to inhibit NF-κB pathway. These results reveal a brain-lung axis involving CRH^{PVN} neurons, pulmonary sympathetic nerves and lung neutrophils that regulate ALI and can be targeted for rapid and effective intervention of ALI in infection and inflammatory conditions.

Fig. 1 | ALI activates CRH^{PVN} neurons. a Schematic diagram of ALI induced by intranasal LPS instillation (20 mg/kg) and brain activity mapping by c-Fos expression in wild-type mice. **b** Representative images of c-Fos expression in the PVN of control (PBS) and LPS-treated mice. Scale bar: 100 μm. **c** Comparison of c-Fos$^+$ neurons in PVN between PBS- and LPS-treated mice (n = 5 mice per group) by a 2-tailed unpaired t-test. **d** Immunofluorescence staining of CRH (red), c-Fos (green), and DNA (blue) in the PVN at 3-h after intranasal LPS administration. Scale bars: 50 μm (low magnification), 20 μm (high magnification). **e** Proportions of CRH$^+$c-Fos$^+$ neurons in total c-Fos$^+$ cells and CRH$^+$ neurons (n = 4 mice). **f** Schematics of fiber photometry detection of neuronal activity in Crh-IRES-Cre mice. **g** Schematic of the mouse brain at Bregma −0.82 mm, adapted from The Mouse Brain in Stereotaxic Coordinates, Second Edition, with permission. A representative image of GCaMP6m fluorescence detected by the positioned optical fiber. Scale bar: 100 μm. **h** Kinetics of the average change of GCamp6m fluorescence (ΔF/F) of CRH^{PVN} neurons in the PBS-or LPS-treated mice. Heatmaps (**i**) and quantification (**j**) of CRH^{PVN} neurons' responses in PBS- or LPS-treated mice (n = 6 mice per group), with statistical difference determined by a 2-tailed unpaired t-test. **k** Schematic of the PRV-531 retrograde tracing experiments in Crh-IRES-Cre mice. **l** Representative of composite images of PRV$^+$ neurons (green) and CRH$^+$ neurons (mCherry, red) in the PVN. Scale bar: 100 μm (left), 50 μm (right). **m** Proportions of EGFP$^+$mCherry$^+$ neurons in EGFP$^+$ cells and mCherry$^+$ neurons (n = 4 mice). Each dot represents an individual mouse. Data are represented as mean ± SEM. **a**, **f**, **k** were created in BioRender. Liu, T. (2025) https://BioRender.com/p48gmjd. All experiments were repeated three times, yielding similar results. Source data are provided as a Source data file. ALI acute lung injury, CRH corticotropin-releasing hormone, LPS lipopolysaccharide, PVN hypothalamic paraventricular nucleus, PRV pseudorabies virus, EGFP enhanced green fluorescent protein.

Results

ALI activates CRH^{PVN} neurons

We employed a mouse model of ALI and ARDS induced by intranasal instillation of lipopolysaccharide (LPS)[15,16] to investigate the role of the brain in regulating lung injury (Fig. 1a). Intranasal instillation of LPS resulted in significant mortality in a dose-dependent manner (Supplementary Fig. 1a). A dose of 20 mg/kg intranasal LPS administration caused considerable lung edema and injury, as indicated by a marked increase in the lung wet-to-dry weight (W/D) ratio and lung injury scores as compared with control mice (Supplementary Fig. 1b–d). By using whole-brain mapping with the neural activity marker c-Fos, we identified six brain regions, including the PVN, that harbored increased numbers of c-Fos$^+$ cells 3 h after LPS exposure, evidencing rapid neuronal activation in these regions (Fig. 1b, c, Supplementary Fig. 2a, b). Dual labeling revealed that nearly 80% of CRH$^+$ neurons were colocalized with c-Fos$^+$ staining, indicating CRH^{PVN} neuronal activation (Fig. 1d, e). To monitor whether CRH^{PVN} neuronal activity was increased in response to intranasal LPS exposure, an adeno-associated virus (AAV-EF1α-DIO-GCaMP6m) expressing a Cre-inducible Ca^{2+} indicator, GCaMP6m, was injected into the PVN of CRH-IRES-Cre mice, and activity-dependent Ca^{2+} fluorescence was measured via an indwelling optical fiber (Fig. 1f, g). Ca^{2+} signals were markedly increased after LPS challenge (Fig. 1h–j), further demonstrating the activation of CRH^{PVN} neurons.

To understand the function of CRH^{PVN} neuronal activation in response to ALI, we first investigated whether CRH^{PVN} neurons in the PVN project efferent signals to the lung. AAV2/9-Ef1α-DIO-mCherry was injected into the PVN of CRH-IRES-Cre mice, where the CRH-specific Cre drives mCherry expression, enabling visualization of CRH^{PVN} neurons. After 3 weeks of full AAV-mediated infection and mCherry expression, we performed a retrograde neuronal circuit tracing by inoculating the lungs of mice with a neurotrophic recombinant pseudorabies virus (PRV) expressing green fluorescent protein (GFP). After 6 days, we observed GFP signal in the spinal cord, brainstem, and hypothalamus (Supplementary Fig. 2c–g, Fig. 1l). In the PVN, abundant CRH neurons also exhibited GFP signal (Fig. 1k–m). These results indicate a neuroanatomical connection between CRH^{PVN} neurons and the lung.

The activation of CRH^{PVN} neurons was further examined using a cecal ligation and puncture (CLP)-induced polymicrobial sepsis model. Similar to the effects of intranasal LPS administration, CLP caused a marked increase in c-Fos$^+$ cells, which are predominantly expressed in CRH neurons at 3-h post-CLP, indicating CRH^{PVN} neuronal activation in response to CLP (Supplementary Fig. 3a–d). The increased calcium activity further confirmed the CRH^{PVN} neuronal activation upon CLP treatment (Supplementary Fig. 3e–g). CRH^{PVN} neuronal activation in response to CLP may be mediated by the nerve transmission or sepsis-related systemic inflammation. Notably, c-Fos activation persisted for up to 24 h following CLP (Supplementary Fig. 4a). Bilateral subdiaphragmatic vagotomy (SDV) effectively blocked the early phase of CRH^{PVN} neuronal activation (1-h post-CLP), suggesting critical involvement of vagal afferent signaling (Supplementary Fig. 4a, b). In contrast, during the later phase (6-h post-CLP and beyond), SDV only mildly inhibited c-Fos upregulation (Supplementary Fig. 4a, b). Combined anti-TNF and anti-IL-1β antibody treatment potently suppressed CRH^{PVN} neuronal activation during this later phase (Supplementary Fig. 4c, d). These results reveal that the activation of CRH^{PVN} neurons in CLP is mediated by neural mechanisms in the initial phase, and primarily driven by systemic inflammation along with neural transmission in the later phase.

CRH^{PVN} neurons activation improves ALI and survival

To investigate whether CRH^{PVN} neurons regulate ALI, we used a chemogenetic approach by stereotactically injecting an excitatory AAV (AAV2/9-Ef1α-DIO-hM3Dq-mCherry, hM3Dq) or control AAV (AAV2/9-Ef1α-DIO-mCherry, Ctrl) into the PVN of CRH-IRES-Cre mice (Fig. 2a). The excitatory DREADD receptor hM3Dq allows for selective activation of CRH^{PVN} neurons upon treatment with clozapine-N-oxide (CNO). CNO treatment effectively activates these neurons, as shown by the co-expression of mCherry and c-Fos 90 min after intraperitoneal (*i.p.*) injection (Supplementary Fig. 5a) and by a significant increase in spontaneous neuronal firing in brain slices (Supplementary Fig. 5b, c).

Whereas a single CNO-induced activation of CRH^{PVN} neurons only demonstrated a trend of improved survival (Supplementary Fig. 5c), sustained activation over 5 days significantly improved survival rates compared to control AAV-injected mice (Fig. 2b), or mice injected with hM3Dq-AAV without CNO activation (Supplementary Fig. 6a). CRH^{PVN} neuronal activation for 2 days markedly attenuated lung injury (Fig. 2c, d, Supplementary Fig. 6b, c), suppressed pulmonary hyperpermeability and edema as evidenced by the reduced W/D ratio of the lung (Fig. 2e, Supplementary Fig. 6d) and lower protein concentrations in bronchoalveolar lavage fluid (BALF) (Fig. 2f, Supplementary Fig. 6e). Furthermore, it substantially suppressed the LPS-induced upregulation of proinflammatory cytokines (IL-1β, IL-6, and TNF) in lung tissue (Fig. 2g and Supplementary Fig. 6f).

Further activation of CRH^{PVN} neurons via the chemogenetic method described above greatly improved survival rate (Supplementary Fig. 7a), and reduced CLP-evoked lung histopathology, lung injury scores, and BALF protein concentrations (Supplementary Fig. 7b–d). Together, these findings show that activation of CRH^{PVN} neurons protects mice against ALI and improves survival.

Inhibition of CRH^{PVN} neurons exacerbates ALI and mortality

We next hypothesized that inhibition of CRH^{PVN} neurons may exacerbate ALI. We injected an AAV carrying an inhibitory DREADD construct, AAV2/9-Ef1α-DIO-hM4Di-mCherry, into the PVN of CRH-IRES-Cre mice (hM4Di) (Fig. 2h). Electrophysiological study showed that CNO treatment dramatically inhibited the spontaneous firing of CRH^{PVN} neurons, confirming successful inhibition of CRH^{PVN} neurons by CNO treatment

https://doi.org/10.1038/s41467-025-63953-7

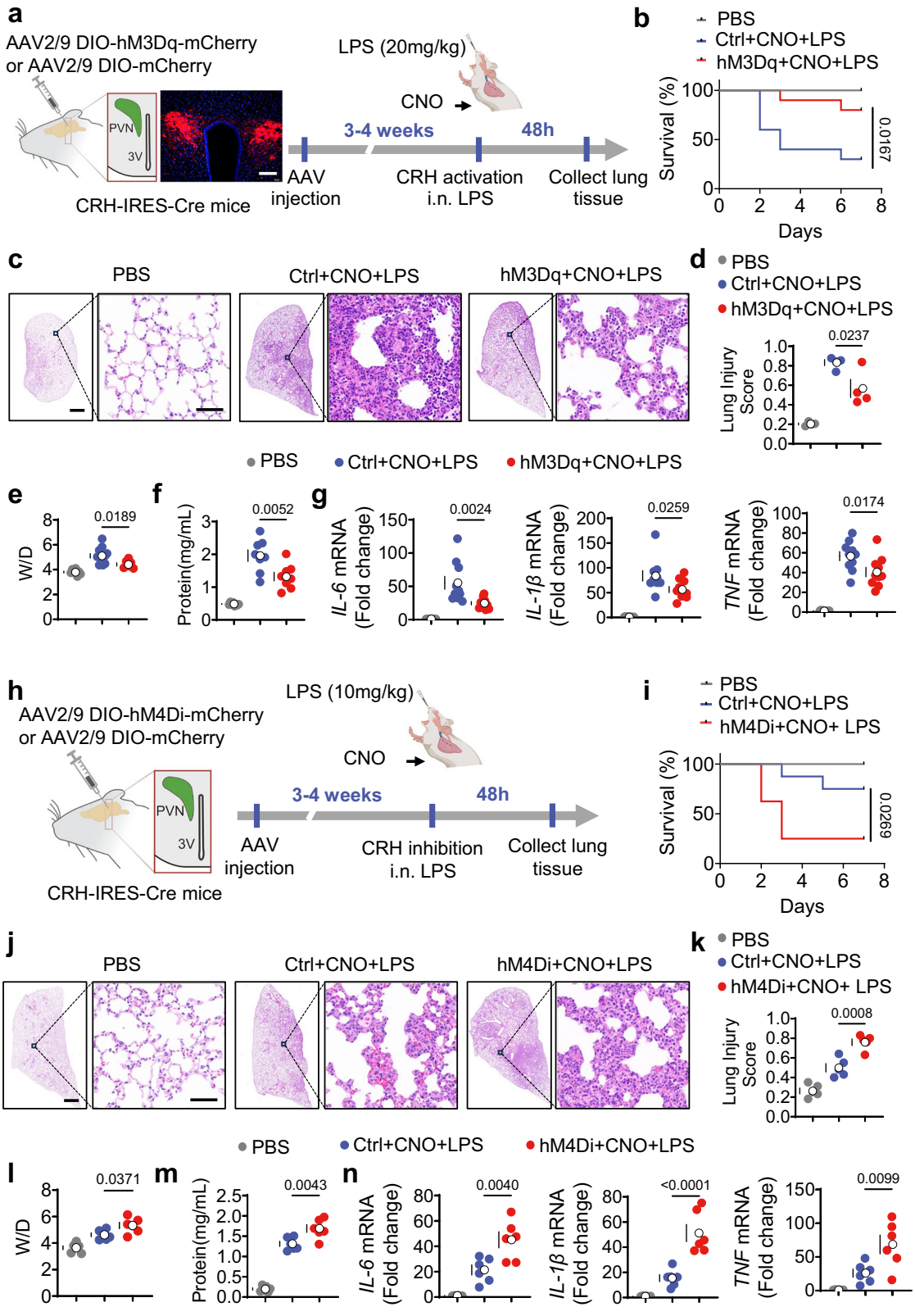

(Supplementary Fig. 8a). Given that 20 mg/kg dose of LPS treatment caused high mortality and may mask the exacerbating effect of CRH^{PVN} neuronal inhibition, we used 10 mg/kg LPS for the CRH^{PVN} neuronal inhibition study. CRH^{PVN} neuronal inhibition with *i.p.* injection of CNO greatly increased the mortality (Fig. 2i, Supplementary Fig. 8b), exacerbated lung inflammation, and increased lung injury scores after ALI as compared with mice injected with control AAV or without CNO treatment (Fig. 2j, k, Supplementary Fig. 8c, d). In addition, inhibition of CRH^{PVN} neurons by CNO worsened pulmonary hyperpermeability and edema (Fig. 2l, m and Supplementary Fig. 8e, f) and amplified the induction of genes encoding IL-6, IL-1β, and TNF in the lung (Fig. 2n and Supplementary Fig. 8g). Therefore, the inhibition of CRH^{PVN} neurons exacerbates ALI.

Fig. 2 | CRH^{PVN} neurons regulate ALI and survival. a Experimental scheme of chemogenetic activation of CRH^{PVN} neurons in CRH-IRES-Cre mice subjected to ALI. Noting the mCherry expression (Red) after AAV injection. Scale bar: 100 μm. **b** Kaplan–Meier survival analysis of control mice and hM3Dq-expressing mice (excitatory DREADD) repeatedly receiving *i.p.* CNO for 5 days following intranasal LPS (n = 10 mice per group). Representative H&E staining (**c**) and lung injury scores (**d**) based on 15 sections per lung of PBS-treated, LPS-treated control, and LPS-treated hM3Dq mice receiving CNO (n = 4 mice per group). Scale bars: 1 mm (low magnification), 50 μm (high magnification). Lung W/D ratio (**e**) (n = 6 mice per group), BALF protein concentration (**f**) (n = 8 mice per group), and IL-6, IL-1β, and TNF mRNA levels (**g**) (n = 10 mice per group) of PBS-treated, LPS-treated control, and LPS-treated hM3Dq mice receiving CNO. **h** Experimental scheme of chemogenetic inhibition of CRH^{PVN} neurons in CRH-IRES-Cre mice subjected to ALI. **i** Kaplan–Meier survival analysis of control mice and hM4Di-expressing mice (inhibitory DREADD) after intranasal LPS exposure (n = 8 mice per group). Representative lung histological sections (**j**) and lung injury scores (**k**) based on 15 sections per lung of PBS-treated, LPS-treated control, and LPS-treated hM4Di mice receiving CNO (n = 5 mice per group). Scale bar: 1 mm (low magnification), 50 μm (high magnification). Lung W/D ratio (**l**) (n = 6 mice per group), BALF protein concentration (**m**) (n = 6 mice per group), and RT-qPCR analysis of IL-6, IL-1β, and TNF mRNA levels (**n**) (n = 6 mice per group) of PBS-treated, LPS-treated control, and LPS-treated hM4Di mice receiving CNO. Statistical differences were determined by the Log-rank (Mantel–Cox) test (**b**, **i**) and 1-way ANOVA with Tukey's *post-hoc* multiple comparisons test (**d**–**g**, **k**–**n**). Each dot represents an individual mouse. Unless specified otherwise, the data are presented as mean ± SEM. **a**, **h** were created in BioRender. Liu, T. (2025) https://BioRender.com/p48gmjd. All experiments were repeated three times, yielding similar results. Source data are provided as a Source data file. ALI acute lung injury, BALF bronchoalveolar lavage fluid, CNO clozapine-N-oxide, CRH corticotropin-releasing hormone, H&E hematoxylin and eosin, W/D wet-to-dry, PVN paraventricular nucleus, RT-qPCR reverse transcription quantitative polymerase chain reaction.

CRH^{PVN} neurons regulate pulmonary neutrophil infiltration and function during ALI

Given the key role of neutrophils in ALI associated with many inflammatory conditions, we analyzed leukocytes, including neutrophils, in the BALF or lung tissues of LPS-treated mice with CRH^{PVN} neurons activation or inhibition[17,18]. Flow cytometry revealed CRH^{PVN} neuron activation significantly reduced the intense infiltration of CD45$^+$ leukocytes and Ly6G$^+$ neutrophils into BALF and lungs, both at 8 h and 48 h following LPS exposure (Fig. 3a–c, Supplementary Figs. 9a–c and 10a–c, g, h), with the percentage of Ly6G$^+$ neutrophils within CD45$^+$ leukocytes unchanged in the lung (Supplementary Fig. 10d, i). In contrast, CRH^{PVN} neurons activation did not significantly affect the number of CD11b$^+$F4/80$^+$ cells in either BALF or lungs at 8 h post-LPS exposure and only slightly reduced their number at 48 h (Supplementary Fig. 9d, e, and Supplementary Fig. 10e, j), with their percentage in lungs increased at 8-h post-LPS instead (Supplementary Fig. 10f, k). Of note, consistent with the flow cytometry data, immunohistochemistry showed that ALI increased the number of lung-infiltrating neutrophils expressing Ly6G and myeloperoxidase (MPO), a component of azurophilic granules able to cause oxidative tissue damage, which was reduced by CRH^{PVN} neuronal activation (Fig. 3d, e). RNA sequencing analysis of lung tissues further showed reduced neutrophil-associated genes and cytokine pathways after CRH^{PVN} neurons activation (Fig. 3f, g and Supplementary Fig. 11).

Conversely, CRH^{PVN} neuronal inhibition by CNO (Fig. 3h) increased the number of CD45$^+$ leukocytes and Ly6G$^+$ neutrophils in both BALF and lung tissues (Fig. 3i, j, Supplementary Fig. 12). This effect was further confirmed by immunohistochemical analysis showing increased Ly6G$^+$ and MPO$^+$ neutrophils in lung tissues (Fig. 3k, l). Collectively, these findings show that CRH^{PVN} neurons play a role in regulating neutrophil recruitment into the lung during ALI.

We further examined whether CRH^{PVN} neurons regulate neutrophil function during ALI by performing RNA sequencing of neutrophils isolated from the lungs of LPS-treated mice following chemogenetic activation of CRH^{PVN} neurons (Fig. 4a). Compared with LPS-treated control mice, CRH^{PVN} neurons activation caused downregulation of 1109 genes and upregulation of 1028 genes in lung neutrophils (Fig. 4b). KEGG analysis revealed that the top pathway included chemokine signaling, oxidative phosphorylation, efferocytosis, NF-κB signaling pathway, and cytosolic DNA sensing, suggesting that activation of CRH^{PVN} neurons exerts multiple effects on lung neutrophils (Fig. 4c). Activation of neutrophils exert several key effector processes, including phagocytosis, the subsequent respiratory burst to produce reactive oxygen species (ROS) and formation of neutrophil extracellular traps (NETs) to kill pathogens, which may also induce collateral tissue damage when hyperactivated. Flow cytometry analysis demonstrated that CRH^{PVN} neuron activation significantly inhibited both phagocytic capacity (as shown by reduced uptake of FITC-labeled latex beads; Fig. 4d) and ROS production (evidenced by decreased DCFH-DA fluorescence intensity; Fig. 4e) in BALF neutrophils of LPS-treated mice. While ALI induced NETs formation in the lung of LPS-treated mice, as indicated by co-staining of CitH3 and MPO, CRH^{PVN} neuronal activation robustly inhibited LPS-induced NETs formation (Fig. 4f, g). Overall, these data show that the activation of CRH^{PVN} neurons restrains the pathogenic functions of neutrophils during ALI.

Lung sympathetic nerves mediate the effect of CRH^{PVN} neurons on ALI via β_2-AR

The sympathetic nervous system (SNS) and the hypothalamic–pituitary–adrenal (HPA) axis are the two major systems that mediate neuroimmune crosstalk of CRH^{PVN} neurons[19–21]. We hence measured the levels of molecules associated with SNS and HPA functions following activation of CRH^{PVN} neurons firstly. Under baseline conditions (AAV-injected mice without LPS challenge), CRH^{PVN} activation significantly elevated the level of plasma corticosterone, an intermediate of the HPA axis. Conversely, in LPS-treated mice, this intervention reduced plasma corticosterone levels (Supplementary Fig. 13a and Fig. 5a). Notably, this neuronal activation consistently increased lung norepinephrine (NE) in both baseline conditions (Supplementary Fig. 13b) and LPS-treated conditions (Fig. 5b), indicating enhanced sympathetic activity. Furthermore, CRH^{PVN} neuronal activation did not result in an increase in the parasympathetic neurotransmitter acetylcholine in lung, suggesting that CRH^{PVN} neurons may not modulate the local parasympathetic nerve activity (Supplementary Fig. 13c). To further assess the effect of CRH^{PVN} neuronal activation on lung SNS activity, we measured the expression of tyrosine hydroxylase (TH), the rate-limiting enzyme in catecholamine synthesis, and found that TH was upregulated in response to CRH^{PVN} activation (Fig. 5c, Supplementary Fig. 13d). Taken together, these data suggest that the protective effect of CRH^{PVN} neurons activation may be mediated by local NE released from the SNS in lung.

To ascertain the role of the lung SNS in this process, we performed chemical sympathectomy via intranasal instillation of 6-hydroxydopamine (6-OHDA), a neurotoxic analog of dopamine, to chemically ablate sympathetic nerves (Fig. 5d). As expected, 6-OHDA administration markedly reduced the TH expression and NE concentration in the lung (Fig. 5e, f). Concomitantly, the protective effects of CRH^{PVN} activation—including survival improvement, attenuated leukocyte infiltration, and reduced protein leakage—were fully abolished by pulmonary sympathectomy following LPS challenge (Fig. 5g–j). Consistent with these findings, mice with CRH^{PVN} neurons activation and treated with 6-OHDA (hM3Dq + LPS + 6-OHDA) exhibited exacerbated lung damage and elevated lung injury scores compared to vehicle controls (hM3Dq + LPS + Veh) (Fig. 5k, l). These results

https://doi.org/10.1038/s41467-025-63953-7

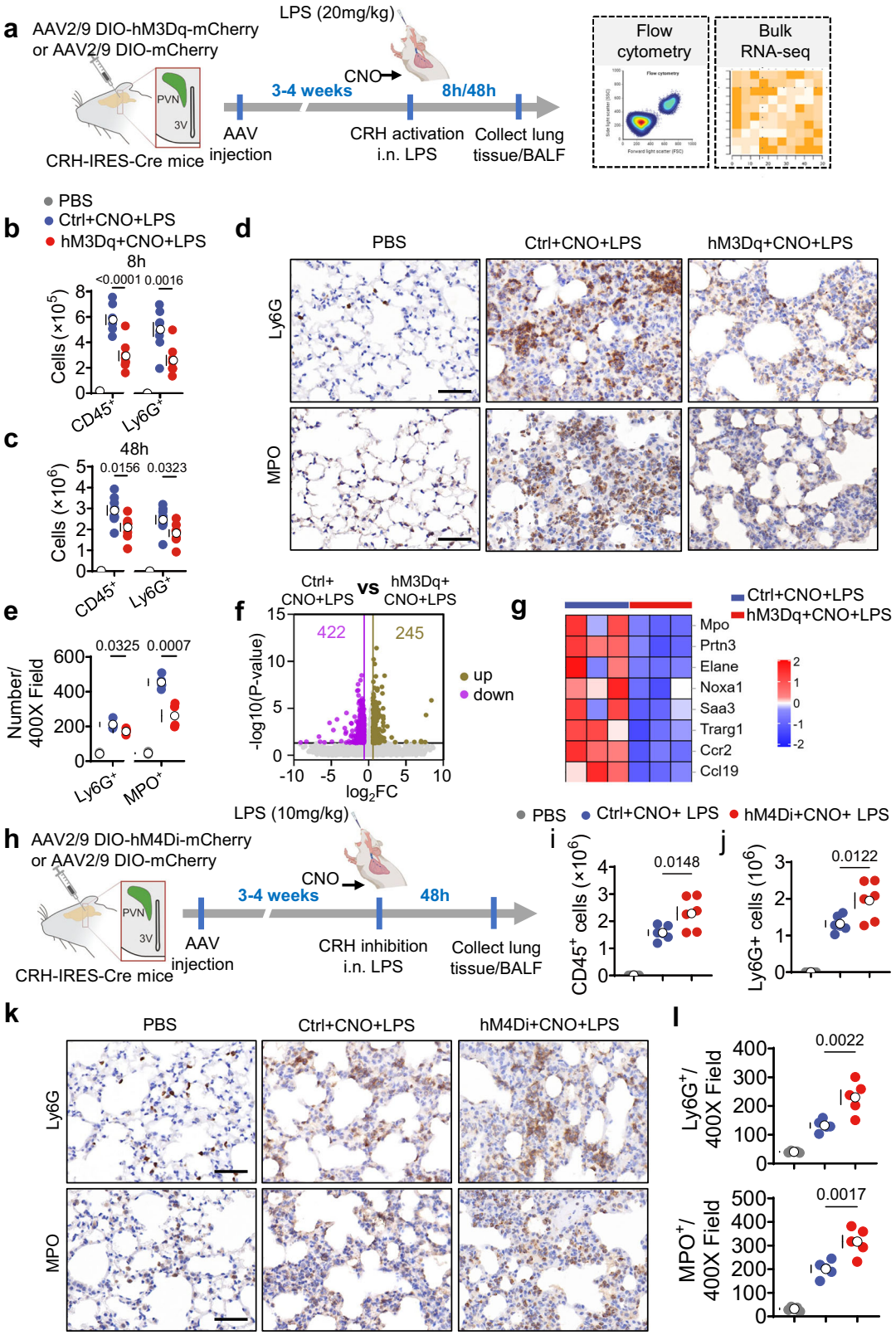

further support the important role of the lung SNS in protection from ALI rendered by activation of CRH^{PVN} neurons.

NE exerts its function through adrenoceptors (ARs), including α-adrenoceptors (α-ARs) and β-adrenoceptors (β-ARs)[22,23]. To investigate the mediators underlying the regulatory function of NE, we analyzed a published lung single-cell sequencing dataset obtained from mice after CLP (GSE207651). β_2-AR, but not β_1-AR, β_3-AR, or α-ARs, was abundantly expressed in neutrophils, and mice subjected to CLP exhibited a higher expression of β_2-AR in the lung than control mice (Supplementary Fig. 14a–h). Consistently, immunostaining revealed that β_2-AR colocalized with $ly6G^+$ neutrophils in the lung (Supplementary Fig. 14i), indicating that local SNS activity may modulate lung neutrophil function through β_2-AR. Indeed, when lung β_2-AR was blocked by intranasal administration of a specific β_2-AR antagonist

Fig. 3 | CRH^{PVN} neurons influence neutrophil infiltration and responses during ALI. a Experimental scheme for chemogenetic activation of CRH^{PVN} neurons in CRH-IRES-Cre mice subject to ALI. Flow cytometry analysis of CD45$^+$ leukocytes and Ly6G$^+$ neutrophils in BALF of PBS-treated, LPS-treated control, and LPS-treated hM3Dq mice receiving CNO after 8 h (**b**) and 48 h (**c**) treatment (n = 8 mice per group). **d** Representative immunohistochemical staining images of Ly6G (upper images) and MPO (lower images) in lung tissues of PBS-treated, LPS-treated control, and LPS-treated hM3Dq mice at 48 h post-LPS challenge. Scale bar: 50 μm. **e** Quantification of Ly6G$^+$ and MPO$^+$ cells in ×400 fields (n = 4 mice per group). **f** Volcano plot of RNA sequencing of lung tissues showing DEGs in control mice and hM3Dq mice subjected to ALI. **g** Heatmap of neutrophil-associated lung DEGs between control mice and hM3Dq mice treated with LPS. **h** Experimental scheme for chemogenetic inhibition of CRH^{PVN} neurons in CRH-IRES-Cre mice subjected to ALI. Numbers of CD45$^+$ leukocytes (**i**) and Ly6G$^+$ neutrophils (**j**) in BALF of PBS-treated mice, LPS-treated control mice, and LPS-treated hM3Dq mice analyzed by flow cytometry (n = 6 mice per group). Immunohistochemical staining (**k**) and quantification (**l**) (in a 400× field) of Ly6G$^+$ and MPO$^+$ cells in the lung of PBS-treated, LPS-treated control, and LPS-treated hM3Dq mice (n = 5 mice per group). Scale bar: 50 μm. Statistical differences were determined by 1-way ANOVA with Tukey's *post-hoc* multiple comparisons test. Each dot represents an individual mouse. Unless specified otherwise, the data are presented as mean ± SEM. **a**, **h** were created in BioRender. Liu, T. (2025) https://BioRender.com/p48gmjd. All experiments were repeated three times, yielding similar results. Source data are provided as a Source data file. ALI acute lung injury, BALF bronchoalveolar lavage fluid, CRH corticotropin-releasing hormone, MPO myeloperoxidase, PVN paraventricular nucleus, DEGs differentially expressed genes.

ICI118551 (Fig. 5m), the protective effect of CRH^{PVN} neuronal activation against ALI was abolished, resulting in the CNO-treated control and hM3Dq-expressing mice having similar numbers of BALF leukocytes and neutrophils, protein levels in BALF, lung histopathology, and lung injury scores after LPS treatment (Fig. 5n–r). These data suggest that the activation of CRH^{PVN} neurons acts through β_2-AR to confer pulmonary protection.

NE regulates neutrophils via β_2-AR–β-arrestin2 signaling to suppress NF-κB pathway

To understand how the lung SNS affects neutrophil function, we examined the effect of NE on neutrophils isolated from bone marrow in vitro (Fig. 6a, Supplementary Fig. 15a). NE treatment markedly decreased LPS-induced phagocytosis (Fig. 6b) and ROS production (Fig. 6c) by these neutrophils. These effects were reversed by butoxamine, a selective β_2-AR antagonist (Supplementary Fig. 15b, c). On the other hand, salbutamol, a selective β_2-AR agonist, inhibited the phagocytosis (Fig. 6d) and ROS production (Fig. 6e) induced by LPS. In addition, NE inhibited the induction of TNF triggered by LPS (Fig. 6f). These results indicated that NE-triggered β_2-AR signals restrain LPS-induced neutrophil responses. RNA sequencing analysis of lung neutrophils from LPS-treated control and hM3Dq-expressing mice revealed NF-κB signaling as a hub modulated by the CRH^{PVN} neurons activation in neutrophils (Fig. 6g). Consistently, NE treatment strongly inhibited p65 and IκBα phosphorylation (Fig. 6h), and translocation of p-p65 into the nucleus in LPS-treated neutrophils (Fig. 6i). β-arrestin2, a β_2-AR-activated negative regulator of NF-κB signaling[23], was upregulated by NE in LPS-stimulated neutrophils (Fig. 6j). In ALI mice, CRH^{PVN} neuronal activation inhibited the upregulation of p-p65 and p-IκBα, and increased β-arrestin2 expression in neutrophils upon LPS exposure (Supplementary Fig. 16). Overall, these results suggest that NE modulates neutrophil effector functions predominantly via the β_2-AR/β-arrestin2-dependent suppression of NF-κB signaling, and that this pathway serves as the mechanism underlying the protective effects of CRH^{PVN} neuronal activation.

Discussion

How the brain perceives and influences lung inflammation remains incompletely understood. Our study demonstrated a role of a brain–lung axis involving CRH^{PVN} neurons, the lung SNS, and neutrophils in sensing and mediating lung immune responses during homeostasis and inflammation. CRH^{PVN} neurons were recently shown to participate in neuroimmune regulation by driving sickness behavior after lung infection[14]. Our study demonstrated that CRH^{PVN} neurons are strongly activated in response to pulmonary inflammatory insult and this activation could provide therapeutic benefit to reduce lung injury and improve survival in such inflammatory conditions. The common effect of CRH^{PVN} neurons activation on sickness behavior and lung protection suggests an adaptive function of sickness behavior upon insult. Indeed, sickness behavior may rapidly exert clinical benefits, such as the enhancement of immune functions and behavioral changes[24–26].

The rapid activation of CRH^{PVN} neurons following respiratory LPS exposure suggests an early adaptive response to acute inflammatory stress. Our findings further demonstrate that short-term activation, including a single stimulation, of CRH^{PVN} neurons can alleviate lung injury, indicating a protective role during the early phase of ALI. However, this transient activation did not significantly improve survival, suggesting that the adaptive response may become compromised over time. Indeed, sepsis patients often exhibit impaired HPA axis function[27–29], which may limit the effectiveness of this neuroendocrine response. Therefore, prolonged activation of CRH^{PVN} neurons appears to be necessary to counteract ongoing systemic inflammation and improve survival. Such activation during ALI or ARDS may help suppress excessive lung inflammation and support the maintenance of lung homeostasis.

Research has shown that mild stress, such as that caused by elevated platform standing, activates CRH neurons and increases adaptive immune functions, such as splenic plasma cell differentiation. In contrast, intensive or persistent stress, such as that caused by prolonged physical restraint, strongly activates CRH neurons without enhancing splenic plasma cell differentiation[30]. These findings suggest that different forms and/or intensities of stress dictate distinct immunomodulatory functions. In our model, CRH neuronal activation exerted major inhibitory effects on neutrophils by dampening their inflammatory responses. The distinct effects of CRH neurons activation on splenic plasma cell differentiation and pulmonary neutrophil function highlight the context- and tissue-dependent nature of brain-mediated peripheral immune regulation.

The effects of neutrophil recruitment to the lung have been extensively studied, especially considering the lung as a major reservoir for neutrophils in various pulmonary diseases, including asthma, ALI and ARDS[31–33]. However, the precise mechanisms by which SNS activity modulates neutrophil function in response to pathological stimuli remain unclear. Our research revealed that NE released by the SNS strongly suppresses neutrophil effector functions, including phagocytosis, oxidative burst, inflammatory response, and NETs formation. Such suppressive effect is underlaid by the abundant expression of β_2-AR in neutrophils of both mice experiencing ALI and patients with ARDS[34–36]. The selective β_2-AR antagonist butoxamine almost completely abolished the suppressive effects of NE on neutrophils, highlighting the critical role of β_2-AR in this process. Signaling through β_2-AR is likely initiated by β-arrestin2, which acts as a signal transducer, linking adrenergic receptors to multiple signaling pathways, such as extracellular regulated kinases (ERK) and NF-κB pathway[37,38]. Consistently, the biological effects of NE were partially mediated by the inhibition of NF-κB, providing mechanistic insight into the complex regulation of neutrophil activity by the SNS in lung diseases.

Our study uncovered a projection of CRH^{PVN} neurons to the lung, suggesting that activating CRH neurons during ALI may provide lung

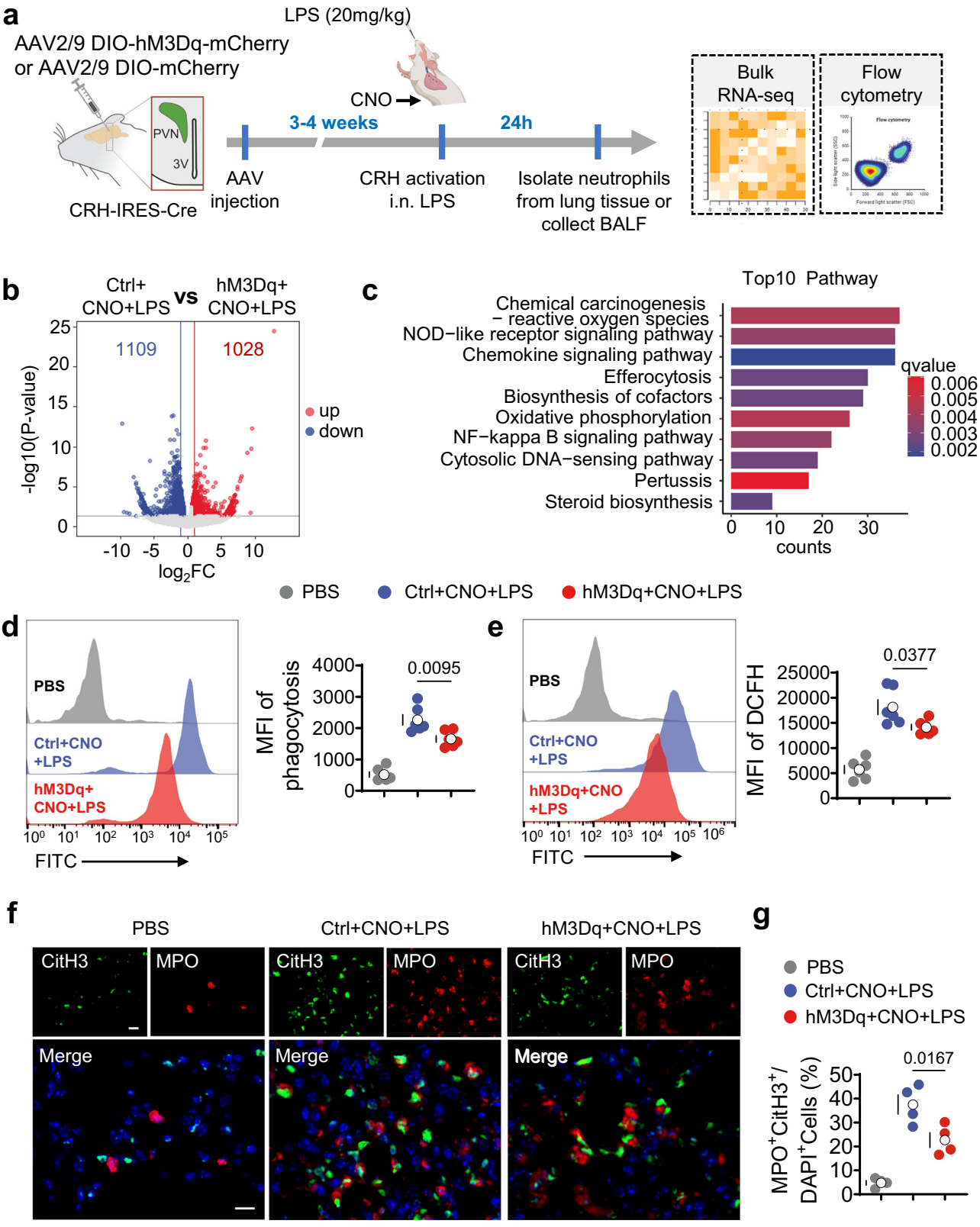

protection by enhancing the activity of the lung SNS. Although the precise synaptic connections remain to be fully elucidated, prior neuroanatomical studies demonstrated that CRH^{PVN} neurons project to sympathetic premotor neurons in the rostral ventrolateral medulla (RVLM) and the intermediolateral cell column (IML) of the spinal cord, which in turn innervate sympathetic ganglia that supply the lungs[39,40]. Consistent with these findings, our retrograde tracing experiments also revealed that the lung receives neural signaling from both the spinal cord, RVLM, and CRH^{PVN} neurons, supporting the hypothesis that CRH^{PVN} neurons project neural signals to the lung, specifically to the lung's sympathetic nerve pathways. Previous work shows that removing sympathetic innervations in the lung enhances LPS-induced recruitment of neutrophil and histopathological damage[41], our findings demonstrate that the CRH neuron–SNS axis having a crucial role

Fig. 4 | CRH^{PVN} activation limits neutrophil effector functions during ALI. **a** Schematic diagram of the experimental procedures in CRH-IRES-Cre mice. Created in BioRender. Liu, T. (2025) https://BioRender.com/p48gmjd. **b** Volcano plot of DEGs identified from neutrophil RNA sequencing data between control mice and hM3Dq mice subjected to ALI. **c** Bar graph of KEGG pathway enrichment analysis from neutrophil RNA sequencing data between control mice and hM3Dq mice treated with LPS. **d** Representative flow cytometry plots and analysis of neutrophil phagocytosis activity of PBS-treated, LPS-treated control, and LPS-treated hM3Dq mice (n = 6 mice per group). **e** Representative flow cytometry plot and analysis of neutrophil ROS production of PBS-treated, LPS-treated control, and LPS-treated hM3Dq mice (n = 6 mice per group). **f** Representative images of NETs in lung tissues of PBS-treated, LPS-treated control, and LPS-treated hM3Dq mice. Scale bar: 20 μm. **g** Quantitative analysis of the percentage of CitH3^{+} neutrophils (n = 4 mice per group). Significance was determined by the 1-way ANOVA with Tukey's *post-hoc* multiple comparisons test. Each dot represents an individual mouse. The data are presented as mean ± SEM. All experiments were repeated three times, yielding similar results. Source data are provided as a Source data file. ALI acute lung injury, CRH corticotropin-releasing hormone, LPS lipopolysaccharide, MFI mean fluorescence intensity, NETs neutrophil extracellular traps, DEGs differentially expressed genes, PVN paraventricular nucleus, ROS reactive oxygen species.

in mediating brain regulation of innate immune responses during ALI. The lung also harbors substantial numbers of neutrophils in many other diseases, such as asthma, cystic fibrosis, and chronic obstructive pulmonary disease (COPD)[33,42–44]. The molecular mechanisms of lung neutrophil regulation revealed by our study may be relevant to these diseases.

There are a number of limitations of our study. First, we focused on CRH^{PVN} neurons in ALI, but the involvement of other brain regions and other PVN neuronal populations cannot be ruled out. Future research should explore their potential contributions to better understand neuroimmune regulation in respiratory infection and pulmonary function. Second, we assessed CRH^{PVN} neurons at certain specific time points after respiratory LPS exposure, which could limit our understanding of their dynamic role throughout ALI progression. While this does not affect our conclusions, long-term studies are needed to evaluate the safety and optimal efficacy of CRH neuron-based interventions. To this end, advances in neuromodulation and behavioral interventions, such as transcranial magnetic stimulation and focused ultrasound, may represent additional treatment options.

In summary, we have uncovered a brain-lung circuitry that senses and regulates lung inflammation by controlling lung neutrophil function via NE-mediated β_2-AR signaling during ALI (Fig. 7). Our study supports this CRH^{PVN} neurons–pulmonary sympathetic nerve–neutrophil axis as a promising therapeutic target amenable to rapid modulation for the treatment of ALI and other pulmonary inflammatory conditions.

Methods

Mice

WT mice (C57BL/6J, 8–10 weeks, male) were sourced from the SLAC Laboratory Animal Co., Ltd (Changsha, China). Adult male CRH-IRES-Cre (Jax 12704) mice were originally from the Jackson Laboratory and maintained on a B6 background. Adult male Crh-IRES-Cre; Ai9 mice, which carry a Cre-dependent tdTomato reporter gene under the control of the CRH promoter, were used for double labeling of c-Fos and CRH^{PVN} neurons, purchased from MouseLab (Wuhan) Biotechnology Co., Ltd.

The mice (*vide supra*) were kept in cages in groups of 4–6 and were housed under specific-pathogen-free conditions at 22 °C–25 °C in a 12-h light-dark cycle. All animal experimental procedures were approved by Institutional Animal Care and Use Committee (IACUC) of the Second XiangYa Hospital of Central South University (No. 20220197) and conducted in strict accordance with the National Institutes of Health "*Guide for the Care and Use of Laboratory Animals.*"

Acute lung injury (ALI) model

To induce acute lung injury, mice (8–10 weeks, male) were anesthetized with isoflurane (3%) and received an intranasal instillation of lipopolysaccharide (*E. coli* LPS O55:B5; Sigma-Aldrich, L2880) dissolved in PBS at 10 mg/kg or 20 mg/kg body weight. For CRH^{PVN} neuronal activation experiments, we used a high LPS dose (20 mg/kg) to establish a severe ALI model to evaluate the therapeutic rescue effects. For CRH neurons inhibition experiments, we reduced the LPS dose to 10 mg/kg to avoid excessive mortality that may potentially mask the exacerbating effects of CRH neuron inhibition. Control mice were administered an equivalent volume of PBS. Following LPS or PBS instillation, animals were returned to their cages and monitored closely for signs of distress or adverse reactions. Mice were sacrificed humanely at predefined time points of 8 h, 24 h, or 48 h post-instillation. Lung tissues and bronchoalveolar lavage fluid (BALF) were collected for subsequent analyses.

Cecum ligation and puncture (CLP) model

Adult male mice were anesthetized with 1% sodium pentobarbital (50 mg/kg). The abdominal area was shaved and disinfected with complex iodine. A 1–1.5 cm midline laparotomy was performed to expose the cecum. The cecum was carefully exteriorized and ligated with a 4-0 silk suture, ensuring that the intestinal continuity was maintained and the blood supply was not compromised. The ligated cecum was then punctured with a sterile 20-gauge needle, and a small amount of fecal content was extruded to ensure perforation. The cecum was repositioned into the abdominal cavity, and the peritoneum and skin were closed with 4-0 sutures.

After surgery, the mice were placed into a clean cage on a heat pad and resuscitated by subcutaneous administration of 1 ml sterile saline to compensate for fluid loss. Sham-operated animals underwent identical procedures, including laparotomy and exteriorization of the cecum, but without cecal ligation or puncture.

Subdiaphragmatic vagotomy (SDV)

Subdiaphragmatic vagotomy (SDV) was conducted as previously described[45,46]. In brief, adult male C57BL/6 mice (20–25 g) were anesthetized with *i.p.* injection of 1% sodium pentobarbital (50 mg/kg). The abdominal area was shaved, disinfected with complex iodine, and a midline incision was made to expose the stomach and esophagus. The vagus nerve was carefully isolated, and both the dorsal and ventral branches along the subdiaphragmatic esophagus were transected using fine forceps. Following surgery, the peritoneum and skin were closed with 4-0 sutures. After surgery, the mice were placed into a clean cage on a heat pad for recovery. In the sham-operated group, the vagus nerve was exposed but not resected.

Stereotaxic injections of viral vectors

Adult male mice were anesthetized with an intraperitoneal (*i.p.*) injection of 1% sodium pentobarbital (50 mg/kg), positioned on a stereotaxic frame, and kept warm with a heated pad.

The skull was adjusted in parallel to the reference panel. Using a microsyringe pump, the adeno-associated virus (AAV) was injected at a rate of 20 nl/min into the paraventricular nucleus (PVN) (AP −0.4 mm, ML ± 0.25 mm, DV −5.0 mm) for pharmacogenetics. The pump was left in position for a further 10 min before removal to facilitate the diffusion and absorption of viral particles at the injection site. The volumes of AAV injected were: AAV9-EF1α-DIO-hM3Dq-mCherry (>2.00E × 10^{12} vector genomes (v.g.)/ml; 120 nl/side), AAV9-EF1α-DIO-hM4Di-mCherry (>2.00E × 10^{12} vector genomes (v.g.)/ml; 120 nl/side),

https://doi.org/10.1038/s41467-025-63953-7

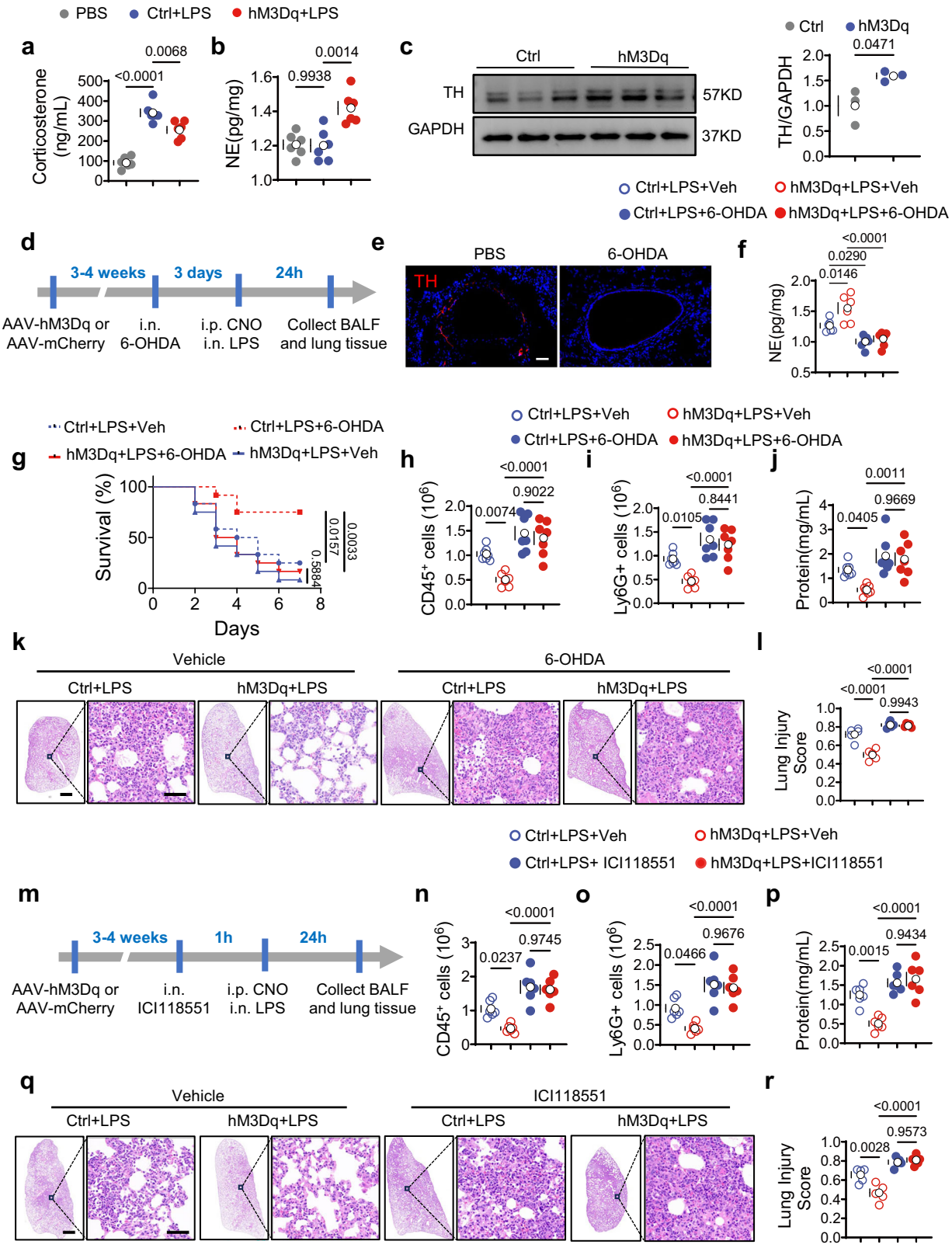

AAV9-EF1α-DIO-mCherry (>2.00E × 10^{12} vector genomes (v.g.)/ml; 120 nl/side).

Fiber photometry

After injection of the AAV-EF1α-DIO-GCaMP6m virus, the optical fiber (outer diameter 125 μm, numerical aperture 0.37) was held in a ceramic clip and inserted into the PVN. Fluorescence signals were acquired using a fiber photometric system equipped with a 470 nm excitation laser. Moreover, a 405 nm laser was concurrently used to isolate the movement-corrected signals from the channel. The laser power was adjusted to minimize bleaching.

Fluorescence signals were recorded before and after intranasal LPS or PBS administration, or CLP. The baseline fluorescence (F_0) was defined as the mean fluorescence value during the 5-min period from

Fig. 5 | CRH^{PVN} neurons regulate ALI through local sympathetic activation. Plasma corticosterone (**a**) and lung NE (**b**) levels of PBS-treated, LPS-treated control, and LPS-treated hM3Dq mice (n = 6 mice per group). **c** Representative western blot and quantification of TH in lung tissue from control and hM3Dq mice (n = 3 mice per group). **d** Schematic of 6-OHDA treatment on CRH-IRES-Cre mice. **e** Representative images of lung TH in PBS- and 6-OHDA-treated mice. Scale bar: 50 μm. **f** Lung NE levels in LPS-treated control and LPS-treated hM3Dq mice with vehicle or 6-OHDA treatment (n = 6 mice per group). **g** Kaplan–Meier survival of LPS-treated control and LPS-treated hM3Dq mice with vehicle or 6-OHDA treatment (n = 12 mice per group). Flow cytometric quantification of CD45$^+$ leukocytes (**h**) and Ly6G$^+$ neutrophils (**i**), and total protein by BCA (**j**) in BALF from indicated groups (n = 7 mice per group). **k** Representative H&E images of the lung. Scale bar: 1 mm (low magnification), 50 μm (high magnification). **l** Lung injury score assessed from 15 sections/lung/mice (n = 5 mice per group). **m** Schematic diagram of ICI118551 (a specific β_2-AR antagonist) treatment on CRH-IRES-Cre mice subjected to ALI. Flow cytometric quantification of CD45$^+$ leukocytes (**n**) and Ly6G$^+$ neutrophils (**o**), and total protein (**p**) by BCA in BALF of LPS-treated control and LPS-treated hM3Dq mice with vehicle or ICI118551 (n = 6 mice per group). Representative lung H&E images (**q**) and lung injury scores (**r**) (n = 5 mice per group). Scale bar: 1 mm (low magnification), 50 μm (high magnification). Significance was determined by 1-way ANOVA with Tukey's *post-hoc* multiple comparisons test (**a**, **b**, **f**, **h**–**j**, **l**, **n**–**p**, **r**), 2-tailed unpaired t-test (**c**), and Log-rank (Mantel–Cox) test (**g**). Data are presented as mean ± SEM. All experiments were repeated three times, yielding similar results. Source data are provided as a Source data file. ALI acute lung injury, BALF bronchoalveolar lavage fluid, CRH corticotropin-releasing hormone, H&E hematoxylin and eosin, LPS lipopolysaccharide, NE norepinephrine, PVN paraventricular nucleus, TH tyrosine hydroxylase, β_2-AR β_2 adrenergic receptor.

−10 to −5 min before surgery. Changes in fluorescence (ΔF/F) were calculated using the formula: $\Delta F/F = (F-F_0)/F_0$, where F is the fluorescence at each time point, and F_0 is the baseline. ΔF/F values were plotted as heatmaps or line graphs, with SEM indicated for visualization. To quantify fluorescence changes, the area under the curve (AUC) was calculated from −5 to 30 min for ALI model, or to 4 h for CLP model. Negative AUC values, which occasionally arise from fluctuations in neuronal calcium signals, particularly in control groups with lower post-model induction activity, were included in the analysis as part of the normal biological variability. Statistical comparisons of AUC values between groups were performed to assess significant differences.

PRV retrograde tracing from the lung

Adult male CRH-IRES-Cre mice were stereotactically injected with AAV9-EF1α-DIO-mCherry into PVN as described above. After 3 weeks, the mice were anesthetized with sodium pentobarbital (1%, 50 mg/kg) and placed on a heated pad in a supine position. After identifying the location of the left lung, 3 μl of pseudorabies virus (PRV-CAG-EGFP, Braincase, PFU/ml) was injected into the left lobe at a rate of 1 μl/min. The syringe was left in position for 5 min after each injection. When the mice were fully awake, they were transferred to the IVC system for careful breeding and real-time status monitoring. Brain, spinal cord, and lung were collected 6 days after injection.

Drug administration

For the 6-OHDA treatment, each adult male mouse was given 500 μg of 6-OHDA (Sigma-Aldrich, H4381) dissolved in 50 μl of sterile PBS that contained 0.1% ascorbic acid (Sigma-Aldrich, A4403) via intranasal injections daily for 3 consecutive days to induce chemical lung denervation. Following the final instillation, mice underwent a 3-day recovery period.

For the specific β_2-AR antagonist ICI-118,551, adult male mice were given 200 μg dissolved in 40 μl of sterile PBS administered by intranasal instillation.

For DREADD-based chemogenetic activation or inhibition, adult male mice expressing hM3Dq, hM4Di, or mCherry were injected with 3 mg/kg clozapine-N-oxide (CNO) *i.p.* (Sigma-Aldrich, C0832). In the survival experiments, adult male mice received once injection of CNO for 5 consecutive days at 24 h intervals to activate CRH neurons, while mice with inhibited CRH neurons received twice-daily injections.

For cytokine neutralization, monoclonal mouse anti-TNF and anti-IL-1β antibodies (BioXcell, Cat No. BE0246 and E0085, respectively) were administered at a dose of 5 mg/kg for each antibody via *i.p.* injection, 1 h prior to CLP surgery as described previously[47].

Bronchoalveolar lavage fluid (BALF)

Mice were anesthetized with 1% sodium pentobarbital. A midline neck incision was made to expose the trachea, and a 1 ml syringe needle was inserted into the trachea, which was then secured with a silk suture.

BALF was performed by instilling 0.5 ml of sterile phosphate-buffered saline (PBS) into the lungs and gently aspirating the fluid. This process was repeated three times to a total of 1.5 ml of PBS. The collected BALF was immediately placed on ice.

Wet/dry (W/D) ratio

The lobe of the right lung of mice was gently separated. Subsequently, the samples were weighed (wet weight), then placed in an oven at 75 °C to dry for 72 h until a constant weight was achieved, and then they were weighed again (dry weight) and the W/D ratio calculated.

Flow cytometry

Single-cell suspensions from BALF or lung tissue were prepared for flow cytometry analysis. For BALF, the fluid was centrifuged at 400 × *g* for 7 min at 4 °C, and the resulting cell pellet was resuspended in 100 μl of PBS. For preparation of the lung single-cell suspension, tissue was minced, mechanically ground, and then subjected to enzymatic digestion. The samples were subsequently centrifuged, and the cell pellet was resuspended in PBS. To prevent non-specific binding, the prepared single-cell suspensions from BALF and lung tissue were incubated with blocking CD16/CD32 antibody (Ab) (BD Biosciences, 553141) for 10 min to block non-specific binding of immunoglobulins. Next, surface staining was performed using Ab against CD45 (BD Biosciences, 30-F11, APC-Cy7), CD11b (BD Biosciences, M1/70, FITC), Ly6G (BD Biosciences, 1A8, PE-Cy7) and F4/80 (BD Biosciences, T45-2342, BV421) for 30 min at 4 °C. Then, 900 μL of RBC lysis/fixation solution (1X, Biosharp) was introduced into each tube, followed by gentle vortex, which was then incubated for 10 min in the dark at 4 °C. Next, 100 μl of Precision Count Beads™ (BioLegend, 424902) was added. Stained cells were read on a flow cytometer (Cystek, Fremont, CA, USA), and the data were analyzed using FlowJo™.

Immunofluorescence and immunohistochemistry

Mice were subjected to transcardial perfusion with 0.9% saline, followed by 4% paraformaldehyde. Brain tissue collected was then post-fixed overnight in 4% PFA and subsequently incubated in PBS with 30% sucrose for 48 h. Sections 20 μm thick were prepared from the brain tissue using a freezing microtome. Lung tissue was embedded in paraffin and sectioned.

For immunofluorescence staining, brain sections were permeabilized/blocked with 0.2% Triton X-100 (PBS-Triton)/5% BSA (Servicebio, GC305006-100 g) solution for 1.5 h at ambient room temperature on a shaker. Primary antibodies were serially diluted with sterile PBS and incubated with brain sections overnight at 4 °C. The primary antibodies were: rabbit anti-c-Fos (1:500, Abcam, ab190289), rabbit anti-CRF (1:100, Abcam, ab272391), mice anti-c-Fos (1:500, Abcam, ab302667), rabbit anti-β_2-AR (1:400, Abcam, ab182136), goat anti-MPO (1:200, R&D Systems, AF3667-SP), rabbit anti-CitH3 (1:200, Abcam, ab5103), rat anti-Ly6G (1:200, BioLegend, 127601), mice anti-TH (1:200, Santa Cruz, Cat# sc-7847), and rabbit anti-β2 Adrenergic Receptor

https://doi.org/10.1038/s41467-025-63953-7

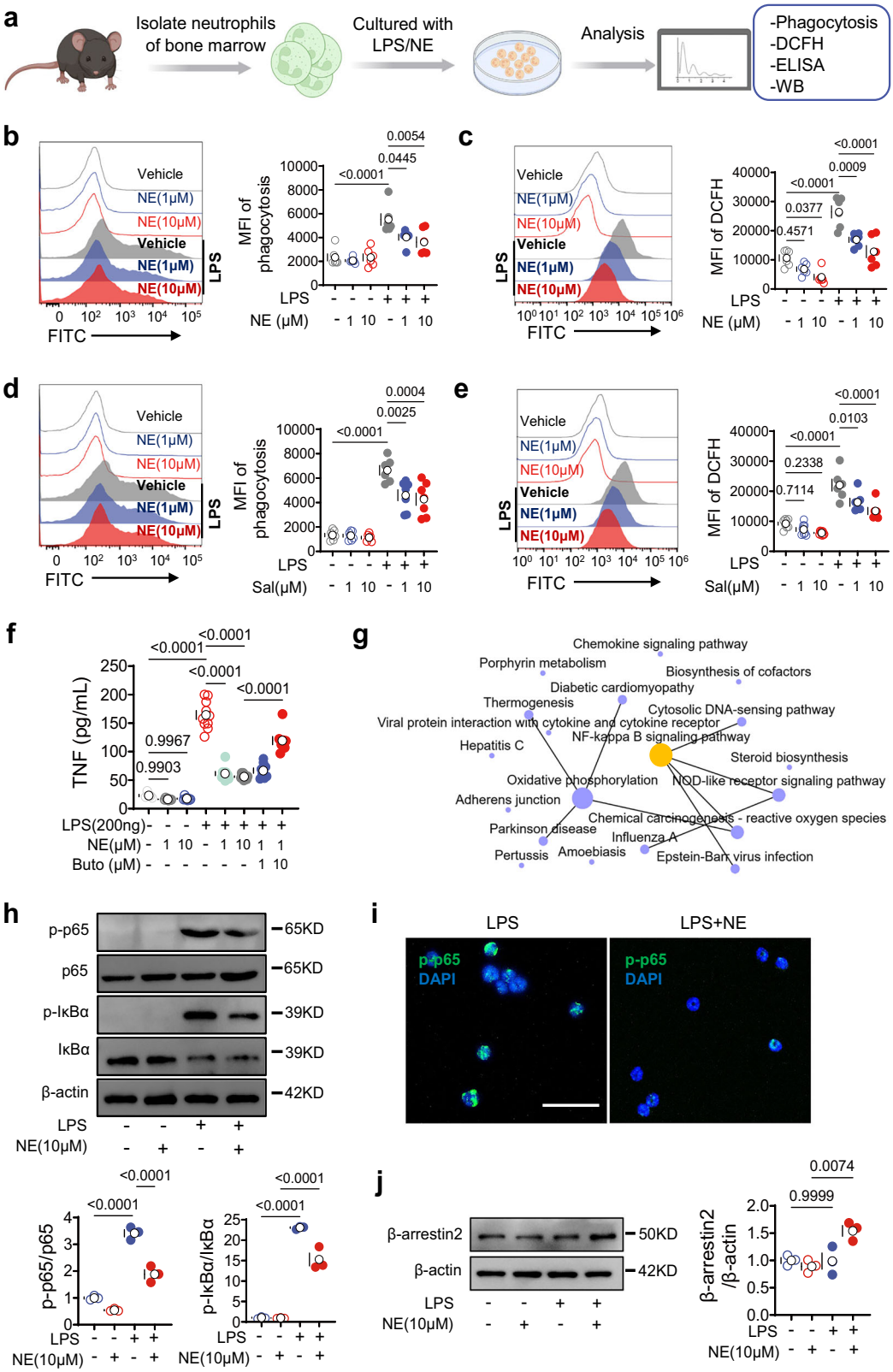

(1:200, Abcam, ab182136). After staining with primary antibodies, the brain sections were washed 3 times in PBS and incubated with Alexa488 Goat anti-Rabbit (1:400, Thermo Fisher, A-11008), Alexa594 Goat anti-Mice (1:400, Thermo Fisher, A-11005), and Alexa594 Goat anti-Rat (1:400, Thermo Fisher, A-11007) for 60 min. After washing, the brain sections were covered by coverslips with DAPI (Southern Biotech, 0100-20). A confocal microscope (NIKON Eclipse Ti) or fluorescence microscope (BX53, Olympus, Japan) was used to take images of the samples.

Immunohistochemistry was performed as previously described[48]. Briefly, lung tissue sections were incubated in 3% H_2O_2 after antigen retrieval. Subsequently, they were permeabilized/blocked with a 0.2% Triton X-100 (PBS-Triton)/5% BSA (Servicebio, GC305006-100 g) solution for 1.5 h at ambient temperature. Primary antibodies,

Fig. 6 | NE regulates neutrophils via β_2-AR–β-arrestin2 signaling to inhibit the NF-κB pathway. a Schematic diagram of the in vitro cell experimental procedure. Created in BioRender. Liu, T. (2025) https://BioRender.com/p48gmjd. **b**, **c** BMNs were treated with NE (1 and 10 μmol/mL) and LPS (200 ng/mL) for 2 h. Neutrophils phagocytosis (**b**) and ROS generation (**c**) were measured by flow cytometry (n = 6 per group). BMNs were pretreated with Salbutamol (1 and 10 μmol/mL) and analyzed for phagocytosis (**d**) and ROS generation (**e**) by flow cytometry (n = 6 per group). **f** TNF concentrations in the cell culture supernatant were measured by ELISA (n = 10 per group). **g** Enriched KEGG pathway interaction networks from neutrophil RNA sequencing data between control mice and hM3Dq mice treated with LPS. **h** Western blot analysis and relative quantities of IκBα, p-IκBα, and p65, p-p65 expression in BMNs with NE or LPS treatment (n = 3 per group). **i** Immunofluorescence staining of p-p65 in BMNs. Scale bar: 20 μm. **j** Representative image and relative quantities of β-arrestin2 in BMNs following NE or LPS treatment (n = 3 per group). Significance was determined by 1-way ANOVA with Tukey's *post-hoc* multiple comparisons test. All experiments were repeated three times, yielding similar results. BMNs bone marrow-derived neutrophils, LPS lipopolysaccharide, NE norepinephrine, ROS reactive oxygen species, β_2-AR β_2 adrenergic receptor, TNF tumor necrosis factor.

including rat anti-Ly6G antibody (1:400, BioLegend, 127601) and rabbit anti-MPO antibody (1:400, Abcam, ab208670), were incubated at 4 °C overnight. Secondary antibodies included: Biotin anti-rat (1:200, Thermo Fisher, 31830) and Biotin anti-rabbit (1:200, Thermo Fisher, 31822), incubated for 60 min. The ABC kit (Vector Laboratories, PK-4000) was incubated at 37 °C for 60 min for subsequent detection. DAB was employed for visualizing positively stained cells.

Histological examination and lung injury score

For histological analyses, the left lung lobes were fixed in 4% neutral formaldehyde and embedded in paraffin. Sections were cut at 4 μm. Hematoxylin and eosin (H&E) staining was used for histological evaluation. Two blinded investigators evaluated H&E-stained histological samples using an established lung injury score[49].

Briefly, 10 random ×400 fields were analyzed according to the following 5 variables: neutrophils in the alveolar space (a); neutrophils in the interstitial space b; hyaline membranes c; proteinaceous debris filling airspaces d; and alveolar septal thickening e. Each variable was given a points score from 0 to 2 points depending on its degree. The lung injury score was calculated thus: Score = [(20 × A) + (14 × B) + (7 × C) + (7 × D) + (2 × E)]/(number of fields × 100), giving a final score between 0 and 1.

Real-time quantitative PCR (RT-qPCR)

Total RNA from lung tissues was extracted using TRIzol Reagent (Thermo Fisher, 15596026) and reverse transcribed using RevertAid first-strand cDNA synthesis kits (TIANGEN, KR123). For the qPCR analysis, the cDNA was utilized as templates along with SYBR Green Master Mix (Novoprotein, E301) using the CFX96 Touch Deep-Well Real-Time PCR Detection System (Bio-Rad Laboratories, Inc.). Primer sequences are shown in Supplementary Table 1. The relative expression of target genes was calculated using the ΔΔCT method with β-actin as the internal reference gene. All qPCR experiments were performed in triplicate, and data are presented as fold changes relative to the control group.

ELISA assays

For corticosterone measurement, the distal end of a mouse tail was amputated to acquire blood plasma. Blood plasma corticosterone concentrations were measured using an ELISA kit (ARBOR ASSAYS, K014-H1) according to the manufacturer's directions.

To analyze NE and Ach concentrations in the lung, 0.5 g of each sample was homogenized in 500 μl of PBS supplemented with 0.01 N HCl, 1 mM EDTA, and 4 mM sodium metabisulfite. Lung NE and Ach concentrations were analyzed using an NE and Ach ELISA kit (Abnova, KA1877 and Elabscience, E-EL-0081, respectively) according to the manufacturer's instructions.

TNF concentrations in the cell supernatant of neutrophils were analyzed with a TNF ELISA kit (R&D Systems, MTA00B) according to the manufacturer's instructions.

Bulk RNA sequencing

Mice received *i.p.* injections of CNO to activate CRH neurons, followed by induction of an ALI model. For lung bulk RNA-seq, mice were dissected, and the left lobe of lung tissue was collected 8 h after modeling. For lung neutrophil bulk RNA-seq, neutrophils in the lung were isolated using magnetic beads (BioLegend, 480058) after 24 h of modeling, as previously described. Those samples underwent RNA sequencing analysis on the Illumina sequencing platform by Genedenovo Biotechnology Co., Ltd (Guangzhou, China). Differentially expressed genes (DEGs) were identified using DESeq with a fold change > 1.5 and a q-value < 0.05. GO analyses were conducted using the "clusterProfiler" package. GO categories were chosen according to their P values.

Single-cell RNA sequencing (scRNA-seq) analysis

The scRNA-seq data (GSE207651) were obtained from the GEO database and filtered using the Seurat package in R4.2.0. Lung samples of CLP mice were clustered as a standard process using the "Seurat" package. Cells that had fewer than 200 UMIs or >20% of their UMI counts derived from mitochondria were classified as low-quality and excluded. Using the parameters "principal components" set to 20 and "resolution" set to 0.5, the "FindClusters" function was employed to detect cell clusters and label each subpopulation based on established biomarkers through a simple analysis and the CellMarker database. The levels of β_1-AR, β_2-AR, and β_3-AR gene expressions were visualized using violin graphs.

Isolation of neutrophils from bone marrow and lung

Bone marrow was flushed from tibiae and femurs through a 27 G syringe with PBS/1% BSA and filtered through a 40 μm cell strainer. Neutrophils were isolated from the collected cells using the MojoSort™ Mice Neutrophil Isolation Kit (BioLegend, 480058) according to the manufacturer's instructions. The isolated neutrophils were assessed by flow cytometry and found to be > 90% pure.

For lung neutrophils, lung tissue was minced and mechanically ground. The resulting cell suspensions were filtered, centrifuged, stained with trypan blue, and counted. After washing with PBS, cells were resuspended and used for neutrophil isolation with a MojoSort™ Mice Neutrophil Isolation Kit (BioLegend, 480058).

Cell culture

Neutrophils sorted from bone marrow (2×10^5 cells/mL) were individually dispensed into 96-well microtiter plates and treated with NE (Selleckchem, S9507), butoxamine (Sigma, B1385), salbutamol (Selleckchem, S5494), or LPS (200 ng/ml) at 37 °C for 2 h. For WB samples, neutrophils were conditioned with NE (Selleckchem, S9507) and LPS (200 ng/ml) for 30 min. The cells were then cultured in a humidified atmosphere enriched with 5% CO_2 at 37 °C.

ROS measurement

The production of ROS in neutrophils was assessed using a DCFH-DA assay kit (Thermo Fisher, 88-5930-74). Neutrophils isolated from bone marrow or cells collected from BALF were treated with 20 μM DCFH-DA to evaluate ROS levels. For BALF samples, the fluid was collected, centrifuged, and the cell pellet was resuspended in PBS before DCFH-DA treatment. Surface staining was performed using antibodies against CD45 (BD Biosciences, 30-F11, APC-Cy7), Ly6G (BD Biosciences,

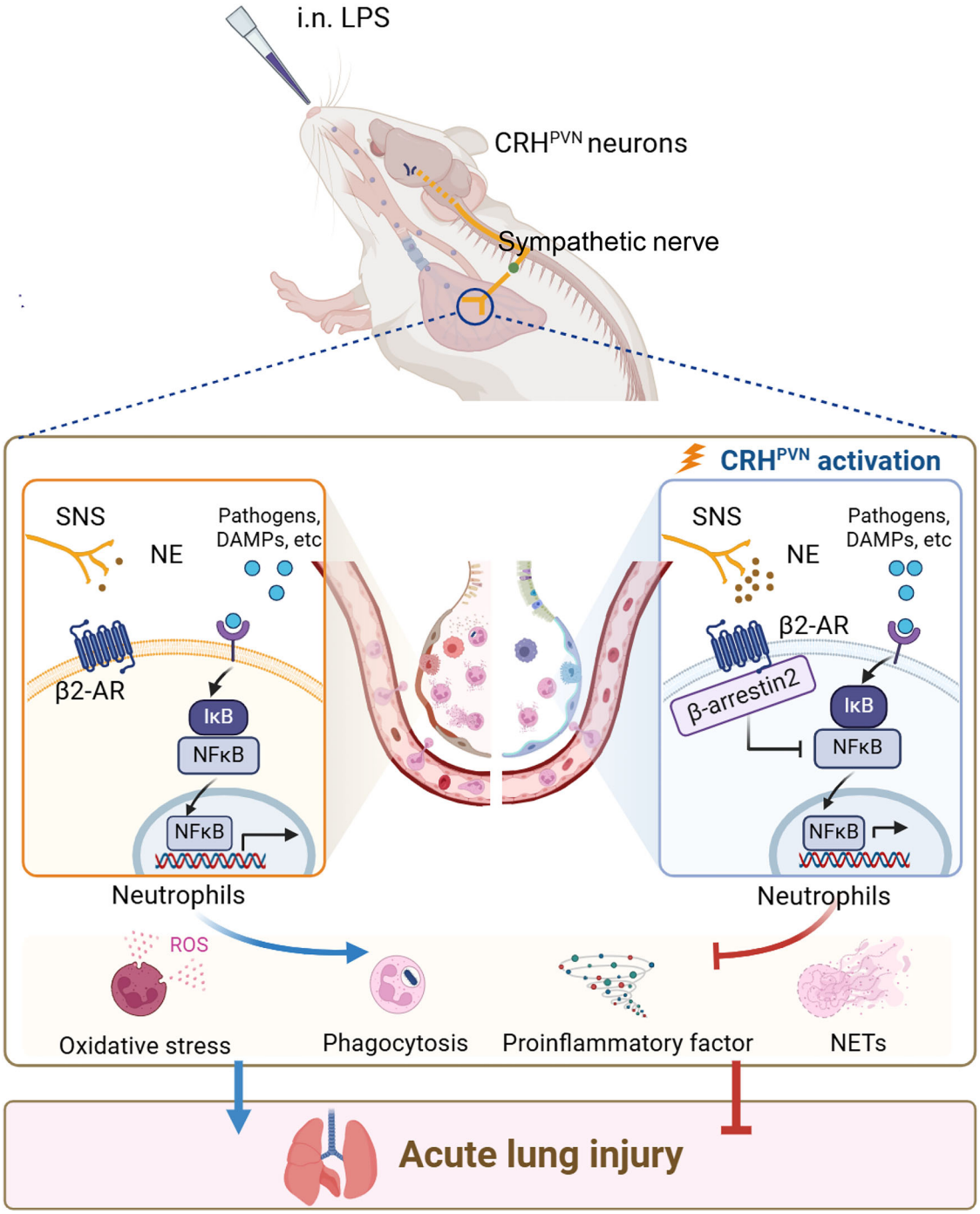

Fig. 7 | Schematic diagram of the mechanism by which CRH^{PVN} neurons activation attenuates ALI. ALI triggers significant activation of CRH^{PVN} neurons. Further activation of CRH^{PVN} neurons stimulates lung SNS and release NE, which limits ALI-induced neutrophils hyperactivities through β_2-AR–β-arrestin2 signaling to suppress NF-κB pathway at least in part. The restrained neutrophils hyperactivities include reducing neutrophil infiltration, inhibiting the production of proinflammatory cytokines and ROS, suppressing the phagocytic function, and NETs formation. Thus, the activation of CRH^{PVN} neurons-lung SNS axis attenuates the progress of ALI and improve mortality. ALI acute lung injury, CRH corticotropin-releasing hormone, SNS sympathetic nervous system, NE norepinephrine, β_2-AR β_2 adrenergic receptor, ROS reactive oxygen species, NETs neutrophil extracellular trap. Created in BioRender. Liu, T. (2025) https://BioRender.com/x91o967.

1A8, PE-Cy7), and F4/80 (BD Biosciences, T45-2342, BV421) to identify neutrophils. Cells displaying positive staining were quantified using a flow cytometer (Cystek, Fremont, CA, USA).

Phagocytic assays

Phagocytosis assays were conducted using a Phagocytosis Assay Kit (Cayman Chemical, 500290). Neutrophils isolated from bone marrow were cultured under different conditions, and FITC-labeled Rabbit-IgG latex beads (1:200) were introduced for a 3-h incubation period at 37 °C. The neutrophils were next washed with 1× PBS and then detected using a flow cytometer (Cystek, Fremont, CA, USA).

Cells obtained from BALF were cultured for 3 h at 37 °C in the presence of FITC-labeled rabbit-IgG latex beads at a dilution of 1:200, washed with PBS and incubated for 30 min at 4 °C with antibodies against CD45 (BD Biosciences, 30-F11, APC-Cy7), Ly6G (BD Biosciences, 1A8, PE-Cy7) and F4/80 (BD Biosciences, T45-2342, BV421). Cells were

then counted using a flow cytometer (Cystek, Fremont, CA, USA). The $CD45^+$ $Ly6G^+$ cells were gated, and the mean of FITC was quantified with FlowJo software.

Western blotting

Extract proteins of lung tissue or neutrophils and then use BCA Protein Assay Kits (Beyotime, P0012) to determine the protein concentration following the manufacturer's protocol. Subsequently, a specific protein quantity was loaded on a 10% SDS-polyacrylamide gel for electrophoresis and then transferred to polyvinylidene difluoride membranes. These membranes were probed with either anti-TH antibody (1:500, Santa Cruz Biotechnology, sc-7847); anti-β-arrestin2 antibody (1:1000, CST, 3857S); anti-IκBα (1:1000, CST, 4812S); anti-Phospho-IκBα (Ser32) (1:1000, CST, 2859S); anti-NF-κB P65 (1:1000, CST, 8242S); anti-Phospho-NF-κB P65 (1:1000, CST, 3033S) anti-GAPDH antibody (1:1000, Abcam, ab8245), and incubated with a HRP-conjugated secondary antibody. The blots were visualized using an imaging system (CLINX, Shanghai, China).

Statistical analysis

Sample sizes were based on prior studies, expected effect size, data variability, and feasibility (ethical use of animals and availability of samples). For in vivo experiments, n = 5–10 animals per group were used. For immunostaining and histological experiments, n = 4–6 animals per group were used. Each sample represents an independent biological replicate, and the exact sample sizes used are provided in the corresponding figure legends.

Data are shown as mean ± SEM. Statistical analysis was performed using GraphPad Prism 8.0 (GraphPad Software, San Diego, CA, USA). To compare differences between two groups, paired or unpaired Student's t-tests were applied as appropriate. For comparisons among more than two groups, one-way ANOVA followed by Tukey's post-hoc multiple comparisons test was used. Survival curves were analyzed using the log-rank (Mantel–Cox) test. Calcium activity changes were analyzed by an unpaired t-test on ΔF/F AUC values. A p value < 0.05 was considered statistically significant. All p values and exact sample sizes are reported in the figure legends.

Reporting summary

Further information on research design is available in the Nature Portfolio Reporting Summary linked to this article.

Data availability

All data are available in the main text or the supplementary materials. The transcriptomics data generated in this study have been deposited in NCBI's Gene Expression Omnibus (GEO) and are accessible through GEO Series accession numbers GSE288588 and GSE288911. In addition, publicly available transcriptomic data from GEO (accession number GSE207651, https://www.ncbi.nlm.nih.gov/geo/query/acc.cgi?acc=GSE207651) were also analyzed in this study. Source data are provided with this paper.

Code availability

The code used in this study is available at: https://github.com/taoge98/scRNA-seq-code and archived at Zenodo: https://doi.org/10.5281/zenodo.16631175.

References

1. McKelvey, M. C. et al. Cathepsin S contributes to lung inflammation in acute respiratory distress syndrome. *Am. J. Respir. Crit. Care Med.* **205**, 769–782 (2022).
2. Li, Y. et al. Central role of myeloid MCPIP1 in protecting against LPS-induced inflammation and lung injury. *Signal Transduct. Target. Ther.* **2**, 17066 (2017).
3. Bos, L. D. J. & Ware, L. B. Acute respiratory distress syndrome: causes, pathophysiology, and phenotypes. *Lancet* **400**, 1145–1156 (2022).
4. Khemani, R. G. et al. Update in Critical Care 2020. *Am. J. Respir. Crit. Care Med.* **203**, 1088–1098 (2021).
5. Hoyer, F. F. et al. Tissue-specific macrophage responses to remote injury impact the outcome of subsequent local immune challenge. *Immunity* **51**, 899–914.e897 (2019).
6. Schappe, M. S. et al. A vagal reflex evoked by airway closure. *Nature* **627**, 830–838 (2024).
7. Azzoni, R., Perdijk, O., Harris, N. L. & Marsland, B. J. Neuroimmunology of the lung. *Annu. Rev. Immunol.* **42**, 57–81 (2024).
8. Gannot, N. et al. A vagal-brainstem interoceptive circuit for cough-like defensive behaviors in mice. *Nat. Neurosci.* **27**, 1734–1744 (2024).
9. Tamari, M. et al. Sensory neurons promote immune homeostasis in the lung. *Cell* **187**, 44–61.e17 (2024).
10. Chen, J., Lai, X., Song, Y. & Su, X. Neuroimmune recognition and regulation in the respiratory system. *Eur. Respir. Rev.* **33**, 240008 (2024).
11. Trevizan-Bau, P. & Mazzone, S. B. Neuroimmune pathways regulating airway inflammation. *Ann. Allergy Asthma Immunol.* **131**, 550–560 (2023).
12. De Virgiliis, F. & Di Giovanni, S. Lung innervation in the eye of a cytokine storm: neuroimmune interactions and COVID-19. *Nat. Rev. Neurol.* **16**, 645–652 (2020).
13. Su, Y. et al. Brainstem Dbh(+) neurons control allergen-induced airway hyperreactivity. *Nature* **631**, 601–609 (2024).
14. Granton, E. et al. Biofilm exopolysaccharides alter sensory-neuron-mediated sickness during lung infection. *Cell* **187**, 1874–1888.e1814 (2024).
15. Burkard, P. et al. A key role for platelet GPVI in neutrophil recruitment, migration, and NETosis in the early stages of acute lung injury. *Blood* **142**, 1463–1477 (2023).
16. Wang, K. et al. Locally organised and activated Fth1(hi) neutrophils aggravate inflammation of acute lung injury in an IL-10-dependent manner. *Nat. Commun.* **13**, 7703 (2022).
17. Song, C. et al. Delayed neutrophil apoptosis may enhance NET formation in ARDS. *Respir. Res.* **23**, 155 (2022).
18. Park, I. et al. Neutrophils disturb pulmonary microcirculation in sepsis-induced acute lung injury. *Eur. Respir. J.* **53**, 1800786 (2019).
19. Elenkov, I. J., Wilder, R. L., Chrousos, G. P. & Vizi, E. S. The sympathetic nerve-an integrative interface between two supersystems: the brain and the immune system. *Pharmacol. Rev.* **52**, 595–638 (2000).
20. Cain, D. W. & Cidlowski, J. A. Immune regulation by glucocorticoids. *Nat. Rev. Immunol.* **17**, 233–247 (2017).
21. Ren, W., Hua, M., Cao, F. & Zeng, W. The sympathetic-immune milieu in metabolic health and diseases: insights from pancreas, liver, intestine, and adipose tissues. *Adv. Sci.* **11**, e2306128 (2024).
22. Thoppil, J., Mehta, P., Bartels, B., Sharma, D. & Farrar, J. D. Impact of norepinephrine on immunity and oxidative metabolism in sepsis. *Front. Immunol.* **14**, 1271098 (2023).
23. Kolmus, K., Tavernier, J. & Gerlo, S. β2-Adrenergic receptors in immunity and inflammation: stressing NF-κB. *Brain Behav. Immun.* **45**, 297–310 (2015).
24. Wang, A. et al. Opposing effects of fasting metabolism on tissue tolerance in bacterial and viral inflammation. *Cell* **166**, 1512–1525.e1512 (2016).
25. Poon, D. C., Ho, Y. S., Chiu, K., Wong, H. L. & Chang, R. C. Sickness: from the focus on cytokines, prostaglandins, and complement factors to the perspectives of neurons. *Neurosci. Biobehav. Rev.* **57**, 30–45 (2015).
26. Bin, N. R. et al. An airway-to-brain sensory pathway mediates influenza-induced sickness. *Nature* **615**, 660–667 (2023).

27. Khardori, R. & Castillo, D. Endocrine and metabolic changes during sepsis: an update. *Med. Clin. North Am.* **96**, 1095–1105 (2012).
28. Leow, M. K. et al. Hypocortisolism in survivors of severe acute respiratory syndrome (SARS). *Clin. Endocrinol.* **63**, 197–202 (2005).
29. Flierl, M. A. et al. Disturbances of the hypothalamic-pituitary-adrenal axis and plasma electrolytes during experimental sepsis. *Ann. Intensive Care* **1**, 53 (2011).
30. Zhang, X. et al. Brain control of humoral immune responses amenable to behavioural modulation. *Nature* **581**, 204–208 (2020).
31. Palmer, C. S. & Kimmey, J. M. Neutrophil recruitment in pneumococcal pneumonia. *Front. Cell. Infect. Microbiol.* **12**, 894644 (2022).
32. Liu, P. Y. et al. RNF128 regulates neutrophil infiltration and myeloperoxidase functions to prevent acute lung injury. *Cell Death Dis.* **14**, 369 (2023).
33. Giacalone, V. D., Margaroli, C., Mall, M. A. & Tirouvanziam, R. Neutrophil adaptations upon recruitment to the lung: new concepts and implications for homeostasis and disease. *Int. J. Mol. Sci.* **21**, 851 (2020).
34. Johnson, M. Effects of beta2-agonists on resident and infiltrating inflammatory cells. *J. Allergy Clin. Immunol.* **110**, S282–S290 (2002).
35. de Coupade, C. et al. Beta 2-adrenergic receptor regulation of human neutrophil function is sexually dimorphic. *Br. J. Pharmacol.* **143**, 1033–1041 (2004).
36. Nicholls, A. J., Wen, S. W., Hall, P., Hickey, M. J. & Wong, C. H. Y. Activation of the sympathetic nervous system modulates neutrophil function. *J. Leukoc. Biol.* **103**, 295–309 (2018).
37. Gao, H. et al. Identification of beta-arrestin2 as a G protein-coupled receptor-stimulated regulator of NF-kappaB pathways. *Mol. Cell* **14**, 303–317 (2004).
38. Li, X. Q. et al. β-arrestin2 regulating β2-adrenergic receptor signaling in hepatic stellate cells contributes to hepatocellular carcinoma progression. *J. Cancer* **12**, 7287–7299 (2021).
39. Stornetta, R. L. & Guyenet, P. G. Distribution of glutamic acid decarboxylase mRNA-containing neurons in rat medulla projecting to thoracic spinal cord in relation to monoaminergic brainstem neurons. *J. Comp. Neurol.* **407**, 367–380 (1999).
40. Geerling, J. C., Shin, J. W., Chimenti, P. C. & Loewy, A. D. Paraventricular hypothalamic nucleus: axonal projections to the brainstem. *J. Comp. Neurol.* **518**, 1460–1499 (2010).
41. Liu, T. et al. Local sympathetic innervations modulate the lung innate immune responses. *Sci. Adv.* **6**, eaay1497 (2020).
42. Ray, A. & Kolls, J. K. Neutrophilic Inflammation in Asthma and Association with Disease Severity. *Trends Immunol.* **38**, 942–954 (2017).
43. Barnes, P. J. Inflammatory mechanisms in patients with chronic obstructive pulmonary disease. *J. Allergy Clin. Immunol.* **138**, 16–27 (2016).
44. Crowley, L. E. et al. Neutrophil dynamics in pulmonary fibrosis: pathophysiological and therapeutic perspectives. *Eur. Respir. Rev.* **33**, 240139 (2024).
45. Chen, J. et al. A vagal-NTS neural pathway that stimulates feeding. *Curr. Biol.* **30**, 3986–3998.e3985 (2020).
46. Zhong, S. et al. Blockade of CCR5 suppresses paclitaxel-induced peripheral neuropathic pain caused by increased deoxycholic acid. *Cell Rep.* **42**, 113386 (2023).
47. Takahama, M. et al. A pairwise cytokine code explains the organism-wide response to sepsis. *Nat. Immunol.* **25**, 226–239 (2024).
48. Zhao, X. P. et al. Early-life sevoflurane exposure impairs fear memory by suppressing extracellular signal-regulated kinase signaling in the bed nucleus of stria terminalis GABAergic neurons. *Neuropharmacology* **191**, 108584 (2021).
49. Matute-Bello, G. et al. An official American Thoracic Society workshop report: features and measurements of experimental acute lung injury in animals. *Am. J. Respir. Cell Mol. Biol.* **44**, 725–738 (2011).

Acknowledgements

This study is supported by the National Natural Science Foundation of China (NSFC) (U24A20684 and 82371292 to R.-P.D.; 82271430 to H.L.), Hunan Provincial Natural Science Foundation (2023JJ30759 to H.L.), and Postgraduate Innovative Project of Central South University (2024XQLH001 to T.L.). We highly appreciate the contribution of Ji Hu (School of Life Science and Technology, ShanghaiTech University) for experiment design and instruction.

Author contributions

R.-P.D. and H.L. conceived, designed, and financed the study. H.L., T.L., X.-M.M., Q.Z., and Y.-Y.X. performed the experiments and analyzed the data. Y.W. and W-Y. S. helped analyze and interpret the data. R.-P.D., H.L., and T.L. drafted the manuscript. K.C. and F.-H.S. discussed data and revised the manuscript. All authors made significant contributions to the manuscript and approved its submission.

Competing interests

The authors declare no competing interests.

Additional information

Supplementary information The online version contains supplementary material available at https://doi.org/10.1038/s41467-025-63953-7.

Correspondence and requests for materials should be addressed to Hui Li or Ru-Ping Dai.

Peer review information *Nature Communications* thanks the anonymous reviewer(s) for their contribution to the peer review of this work. A peer review file is available.